Deep Learning Application for Urban Change Detection from Aerial Images

Tautvydas Fyleris[1], Andrius Kriščiūnas[2], Valentas Gružauskas[3] and Dalia Čalnerytė[2]
[1]*Kaunas University of Technology, Faculty of Informatics, Department of Software Engineering, Lithuania*
[2]*Kaunas University of Technology, Faculty of Informatics, Department of Applied Informatics, Lithuania*
[3]*Kaunas University of Technology, School of Economics and Business, Sustainable Management Research Group, Lithuania*

Keywords: Urban Change, Aerial Images, Deep Learning, JEL: O18, C45, C55.

Abstract: Urban growth estimation is an essential part of urban planning in order to ensure sustainable regional development. For such purpose, analysis of remote sensing data can be used. The difficulty in analysing a time series of remote sensing data lies in ensuring that the accuracy stays stable in different periods. In this publication, aerial images were analysed for three periods, which lasted for 9 years. The main issues arose due to the different quality of images, which lead to bias between periods. Consequently, this results in difficulties in interpreting whether the urban growth actually happened, or it was identified due to the incorrect segmentation of images. To overcome this issue, datasets were generated to train the convolutional neural network (CNN) and transfer learning technique has been applied. Finally, the results obtained with the created CNN of different periods enable to implement different approaches to detect, analyse and interpret urban changes for the policymakers and investors on different levels as a map, grid, or contour map.

1 INTRODUCTION

Urban planning is an essential economic activity for regions seeking to maintain prosperity. It is essential to identify urban growth patterns to be able to provide recommendations for infrastructure planning. One approach might be waiting for an area to expand and plan the infrastructure later; however, in this case, the cost of the projects might increase. An alternative approach could be estimating future urban growth patterns and planning infrastructure projects in advance. Proper preparation for such projects could increase the sustainability of the region in terms of social benefit and economic growth potential. In addition, the identified urban growth patterns can also be used by private companies to plan investment strategies, not limiting to government institutions. Urban growth analysis can be conducted using different data sources and methodologies. For instance, social-economic indicators of the region could be analysed to estimate the demographic change. However, this kind of data mainly focuses on the temporal aspects, with a limited focus on spatial ones. Thus, for urban growth analysis, remote sensing data can be used more effectively. Remote sensing data consists of satellite images, radar images, aerial images, etc. A comprehensive overview of remote sensing data for economics has been provided by (Donaldson & Storeygard, 2016). To detect change in remote sensing data, mainly two approaches are used.

One approach is unsupervised learning, which focuses on change detection of pixels without clearly identifying the types of detected objects. Similar applications have been conducted in video analysis, which focuses on unsupervised learning, i.e. change of individual pixels, rather than recognition of the specific object. Goyette et al. (2012) created a dataset for testing change algorithms in videos. This dataset has been widely used to develop algorithms (Goyette et al., 2012). Kanagamalliga and Vasuki (2018) proposed a video flow analysis approach, in which firstly the background is extracted and later the contour of the movable object is determined (Kanagamalliga & Vasuki, 2018). Wang et al. (2019) developed a motion tracking algorithm based on tubelet generation, which compares the change in frames to improve the video object detection (B. Wang et al., 2019). Similar approaches have been previously developed to evaluate change and monitor the disturbances in satellite images based on vegetation index, which is suitable for disaster monitoring (Verbesselt et al., 2010; Verbesselt et al., 2012). Similar change detection methods have also

Fyleris, T., Kriščiūnas, A., Gružauskas, V. and Čalnerytė, D.
Deep Learning Application for Urban Change Detection from Aerial Images.
DOI: 10.5220/0010415700150024
In *Proceedings of the 7th International Conference on Geographical Information Systems Theory, Applications and Management (GISTAM 2021)*, pages 15-24
ISBN: 978-989-758-503-6

been tested with satellite images. For example, Celik (2009) proposed principal component analysis and k-mean clustering to develop an unsupervised change detection algorithm (Celik, 2009). Jong and Bosman (2019) developed an unsupervised change detection algorithm by using convolutional neural networks (de Jong & Sergeevna Bosman, 2019).

Another approach is to use supervised learning and detect precise objects from remote sensing data, such as roads, buildings, forests, etc. For example, Wang et al. (2015) proposed a deep learning approach to extract road networks from satellite images (J. Wang et al., 2015). Nahhas et al. (2018) developed a deep learning approach for building detection in orthophotos (Nahhas et al., 2018). Langkvist et al. (2016) integrated satellite images with digital surface models to improve per-pixel classification of vegetation, ground, roads, buildings, and water (Längkvist et al., 2016). Marmanis et al. (2016) developed a deep learning algorithm for aerial image classification with a 88.5% accuracy (Marmanis et al., 2016). Transfer learning is also widely applicable in remote sensing area. Xie et al. (2016) extracted light intensity of satellite images, validated the approach with respect to the survey data, used transfer learning to train the model on known data and applied it to estimate poverty levels in Uganda (Xie et al., 2016). Wurm et al. (2019) used a similar approach of transfer learning to estimate slums. The initial model was trained on high quality satellite images of QuickBird and transferred to Sentinel-2 images, which allowed for gaining higher accuracy in estimating slums (Wurm et al., 2019). After identifying the objects in remote sensing data, they can be combined with various social-economic indicators, thus reducing the costs of surveys. Jean et al. (2016) developed a machine learning approach to predict poverty from satellite images. The approach integrated the deep learning model with survey data, which helped reduce the costs and increase the accuracy of social demographic indicators (Jean et al., 2016). Suraj et al. (2018) developed a machine learning algorithm to monitor the development indicators from satellite images (Suraj et al., 2018).

In summary, it can be stated that most of the publications focus on detection of specific object at a micro level in high resolution images. For the lower resolution images (e.g. Copernicus), research is mainly conducted on recognition of the type of land use (e.g. agriculture land). Usually these images are integrated with radar images and focus on reflection analysis. Only a limited number of studies been identified, in which analysis for a time-series of images at a country level is performed. In most of them, limited information on the methodological approach and possible issues is provided. Thus, our publication focuses on filling this gap.

In this publication, we focus on extraction of indicators from a time series of visual information in relation to geospatial data. The difficulty in analysing a time series of remote sensing data lies in ensuring that the accuracy stays stable in different periods. For instance, if one period of aerial images has an accuracy of 90%, and another of 86%, it would be unclear whether the urban change actually happened, or it was calculated due to the error of the machine learning (ML) model. Thus, it is important to ensure consistent accuracy of object detection between different periods. In this paper, the available dataset of the same geographical region in different time periods was of different quality due to the image spectrum and resolution. This was caused by the fact that with time, technical capabilities enabled attaining better quality (i.e. before 2000, visual data for the same region was available only in grey scale compared to the current RBG of 16 bit depth). Moreover, the ground truth data may vary due to the time delay between the real actions, which are visible in real time and data input to registers or external databases. To overcome these limitations, transfer learning technique has been applied. The initially pre-trained DeepLabv3 model with a ResNet50 backbone trained on the ImageNet data has been selected. Next, model adjustment has been carried out in two steps, with coarse and fine-tuning datasets. The coarse dataset was created automatically by randomly selecting different locations and merging it with the labels of Open Street Map. The fine-tuning dataset was created according to the same principles; however, the images were manually reviewed by removing those, for which the labelled data did not meet the actual visible data. Finally, to ensure that the model of different periods provides similar accuracy, we normalised all datasets according to the one of the worst quality (oldest in time) and the fine-tuning operation for different time periods was performed for separate models, where loss behaviour was tracked for the sub-model of each period. Incidentally, such strategy allows to better adapt each sub-model for the variances of photo in different periods, i.e. seasons, times of the day, etc. Afterwards, results obtained with the created ML model of different periods will enable to implement different approaches to detect, analyse and interpret urban changes for policy makers and investors. This means that the approaches used to analyse the parsed data may be applied on different levels, i.e. on the finest level, the processed data can be seen as a map.

Figure 1: Example of view difference at the same place in different periods.

On the middle level, the difference of the indicator can be analysed to easily detect the change of the selected indicator in grid cells and their clusters. On the highest level, the change of the indicator can be presented as a contour map.

2 METHODOLOGY AND DATA ANALYSIS

2.1 Methodology Overview and Selection of Dataset

The idea that urban changes in time can be determined by the view visible in aerial photos is demonstrated by the example, where the number of buildings at same place differs (see **Fig 1**).

A different speed of changes of buildings, forests, land use, etc. in the regions may result in different development speed of the region. Visual data of Lithuania has been selected for the analysis of the relationship between the information obtained using computer vision to track and interpret the visual information (raster graphics). The research focuses on two main objectives:

a) to create a machine learning (ML) model, which enables to obtain interpretable values on the country level in different time periods and to analyse them on a granular level;
b) to perform an analysis of the ML model results according to its suitability for the identification of different urban growth patterns.

Different data sources for analysis have been investigated. Firstly, Copernicus Sentinel Missions was considered as a data source. However, after serious consideration it yielded the following problems:

- low resolution for building segmentation and initial tests demonstrated bad results;
- only recent data is stored, and historical data is not available.

Admittedly, there are several methods to improve the model accuracy, e. g. Shermeyer and Etten (2019) applied super-resolution to satellite images and concluded that super-resolving native 30 cm imagery to 15 cm yielded the best results of 13 – 36% improvement when detecting objects (Shermeyer & Van Etten, 2019). The image can be also enhanced using a discrete wavelet transform as was done in the study of Witwit et al. (2017) (Witwit et al., 2017). Furthermore, studies have been conducted where Sentinel 2 data was used to classify the building areas of the ground (Krupinski et al., 2019), (Corbane et al., 2020); however, due to a wider period of data and better quality, ORT10K was chosen as an alternative source for this study. The first period data resolution of ORT10K was 0.5 m x 0.5 m and 8 bit RGB depth (7 bit effective), for the second and third periods, image resolution increased to 0.25 m x 0.25 m per pixel, while the colour depth for the second period was 8 bit RGB and 16 bit for the third. The principal scheme of the research is shown in **Fig. 2.** The detailed steps of analysis are described in the following chapters.

2.2 Computer Vision Model

Dataset Preparation and Normalisation. The ORT10LT contains 3 periods of country-specific visual information. For labelling (indicators), the Open Street Map (OSM) data source was chosen as ground truth. Automatic query OSM database was used for labelling. Technically, the process can be described as follows: the ORT10LT segments were cut by the chosen geographic points in the country and then labelled directly from the OSM database (**Fig. 3**).

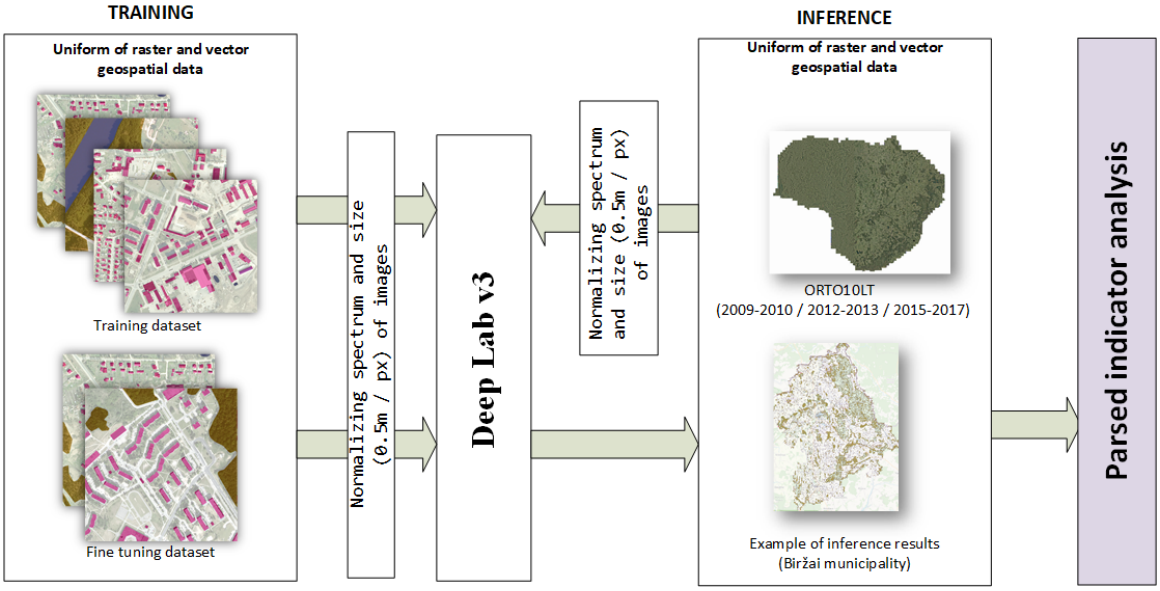

Figure 2: Principal scheme of the ML model construction and extraction of interpretable indicators.

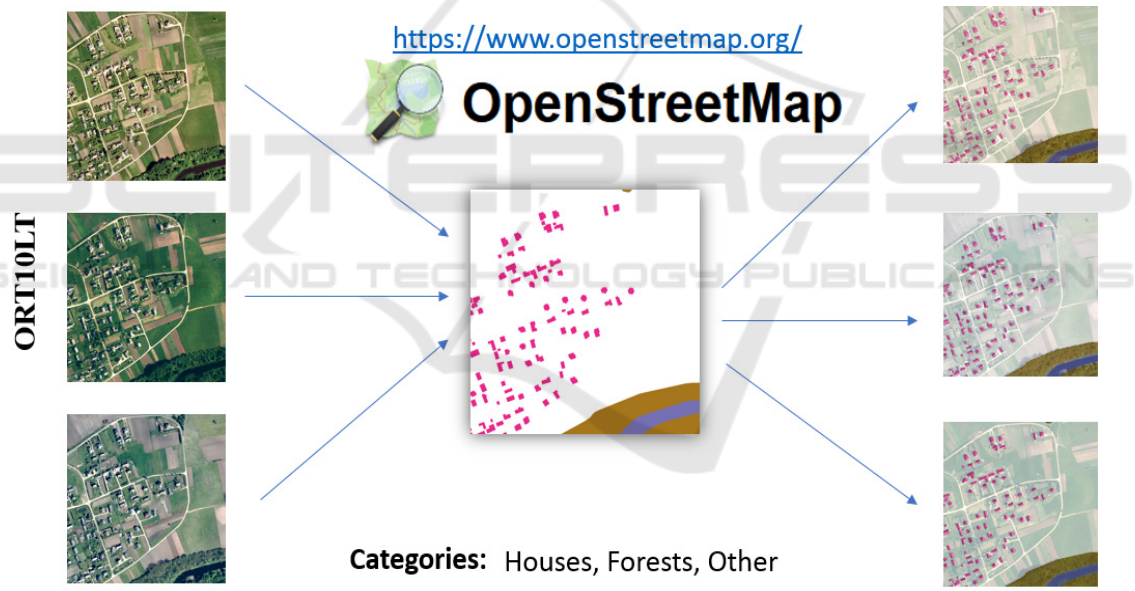

Figure 3: Dataset preparation.

The OSM data has a lot of categories; however, in this research, only 3 categories have been selected: houses, forests and other. Water and road categories have also been considered for inclusion into the model, but due to the fact that the photos were taken in different seasons (spring/summer), it was concluded that the river flood might affect the water area significantly. Moreover, while using RGB only, water in some regions can be hard to distinguish from vegetation (green water). The road category was left out due to the fact that OSM mapping data defines roads only as lines (not polygon): although the width of the road can be technically guessed from the data, it is not always correct. Finally, following the dataset analysis, two types of problems were identified in the selected dataset:

- ***logical*** – the OSM data does not always match the photos due to mistakes in mapping or changes in the environment;
- ***quality*** – the results for photos taken in different periods or locations may vary due to their quality:

a b c d

Figure 4: a, b) image selected with a house centred; c, d) image selected randomly.

(a) images were taken at a different time of the day, which results in varying lighting (early morning vs noon);
(b) subtle angle differences between photos;
(c) the equipment used to capture the images in different location differs (different colour response and dynamic range; the captured images are blurry due to the fact that the photos were taken early in the morning or at night).

The ***logical*** problem has been solved in the dataset preparation stage. The training dataset image size chosen was 1024x1024 pixels (the main constraint being the GPU memory limit). To avoid the initial bias in the dataset distribution, when e.g. only rural areas are selected for the initial training dataset, the dataset was prepared according to the indicators (houses, vegetation), which would be analysed in the next stage. The first part of the dataset was created by picking a random building from the OSM database and focusing it in the middle of the input image. The second part was constructed by applying the same technique where random points for the whole country have been selected. Finally, for the coarse dataset, 5,000 images have been selected (4,000 with buildings and 1,000 with vegetation, covering a total area of 1,250 km^2). Different techniques of initial image selection and a relatively large number of images allow for ensuring that different cases are covered for the whole country dataset. Examples of different parts are provided in **Fig. 4.**

The fine-tuning dataset was created according to the same principles; however, the images were manually reviewed by removing the ones, for which the labelled data did not meet the actual visible data. Ultimately, 320 images (210 with buildings and 110 with vegetation, covering a total area of 80 km^2) were selected.

To solve the problems related to the different quality of images, normalisation procedure was used as follows:

a) resolution was normalised to 0.5 m/pixel;
b) contrast was normalised using a 2%–98% percentile interval; all pixels over and under the interval were clipped to minimum or maximum values;
c) standard computer vision normalisation procedure was applied (mean=[0.485, 0.456, 0.406], std=[0.229, 0.224, 0.225]).

Model Training and Result Analysis on the Finest Level. Various models and visual analysis methods can be used for object detection, segmentation, or instance segmentation (Längkvist et al., 2016; Liu et al., 2020; Marmanis et al., 2016; Wurm et al., 2019). The argumentation for selecting the model deals with the computational restriction to be able to analyse the whole country in different periods. For this reason, DeepLab3 with a ResNet50 backbone was chosen (the main prerequisite being to be able run on limited VRAM devices: NVIDIA RTX 2080ti with 11GB RAM). The loss function was changed from Softmax entropy loss to focal loss (Corbane et al., 2020) due to the nature of data, absence of labels and mislabelled areas (for example, areas without buildings, or just background). Focal loss is an alternative approach to loss function, which focuses on misclassified examples and imbalanced data (such as representing a single class in the entire detection region, for example, forest only) and yields good practical results. Formally, focus loss $FL(p_t)$ can be defined by the following equation:

$$FL(p_t) = -\alpha(1-p_t)^{\gamma} log(p_t) \quad (1)$$

where α is for α - balanced form to reduce impact for detection outliners; γ – is the focal factor. When γ = 0, focal loss is the same as cross-entropy loss; however, with higher γ values, the loss reduces the impact of easy examples and scales down the total

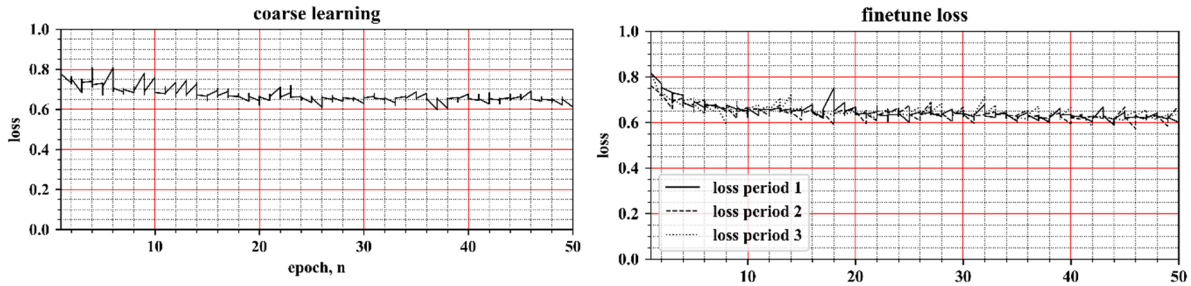

a b

Figure 5: a) coarse learning loss; b) fine-tuning losses for 3 periods using fine-tuning.

loss value, which in turn increases the probability of correcting misclassified examples. The class classification function p_t has the following definition:

$$p_t = \begin{cases} p & if y = 1 \\ 1 - p & otherwise \end{cases} \quad (2)$$

where y specifies the ground truth class $y \in \{\pm 1\}$ and $p \in [0,1]$ is the model probability for the class. For this experiment, α =0.25 and γ =2.

The technical specifications of the selected model are as follows:

- input layer: 1024 x 1024 pixels (result taken from 896 x 896 pixels) ~ 448 m x 448 m (or ~0.2 km^2) area;
- coarse learning: learning rate 0.5e-3; momentum 0.5; 5,000 samples per epoch;
- fine-tune: learning rate 5e-05; momentum 0.1; 100 samples per epoch.

The mean value of focal loss (1) during the training process of the model is provided in **Fig 5**

From the training process (see **Fig. 5.**) it can be seen that the initial model with the coarse dataset converges slower compared to models with the fine-tuning dataset. Furthermore, all models for the fine-tuning operations start from a similar loss function value and correspond to the initial one of the coarse dataset. It could be explained by the fact that errors in the test vector of the coarse dataset compared to the correctly labelled parts do not outweigh the errors in different periods. In addition, it can be clearly seen that the single model for each time period works better with the fine-tuning dataset, for which the incorrectly labelled data has been removed. Such model separation strategy for each period provides two valuable properties. On the one hand, if, in the model training process, the image quality normalisation process between periods leaves some shortcomings and the image still has differences due to its technical quality or seasonality between the periods, then the model adapts easier to the photo specifics, the dataset necessitating revision for the model training is smaller, and better final results can be obtained. On the other hand, the model training results can be compared between different periods to validate that models work well for different periods and provide similar results, which allow for comparison of results of different time periods. In case of a bias of building detection between periods, the quality of normalisation should be taken into account, or correction coefficients could be applied to minimise the bias.

3 ANALYSIS OF RESULTS

Finally, the model has been developed using 3 main indicators. The direct results obtained with the developed model of different periods enabled to analyse and interpret the results on different levels. Firstly, the analysis of urban change could be conducted on the country level.

The buildings detected in the aerial images can be depicted as polygons scattered through the region. From this information, it is possible to create a plot for spatial distribution by using kernel density. **Fig. 6.** shows the kernel distribution of buildings identified in the last period of images (year 2015 – 2017). The figure represents the whole Lithuania, which area is 65,300 km². The distribution clearly identified the major cities of Lithuania, i.e. Vilnius, Kaunas, Klaipėda, Panevėžys, and Šiauliai.

On the middle level, it is possible to identify more clearly the change of the region by creating a heat map. For the creation of the heat map, the country was divided into a grid, with the identification of the total number of buildings detected per grid. Then, the difference between the periods and grids was obtained.

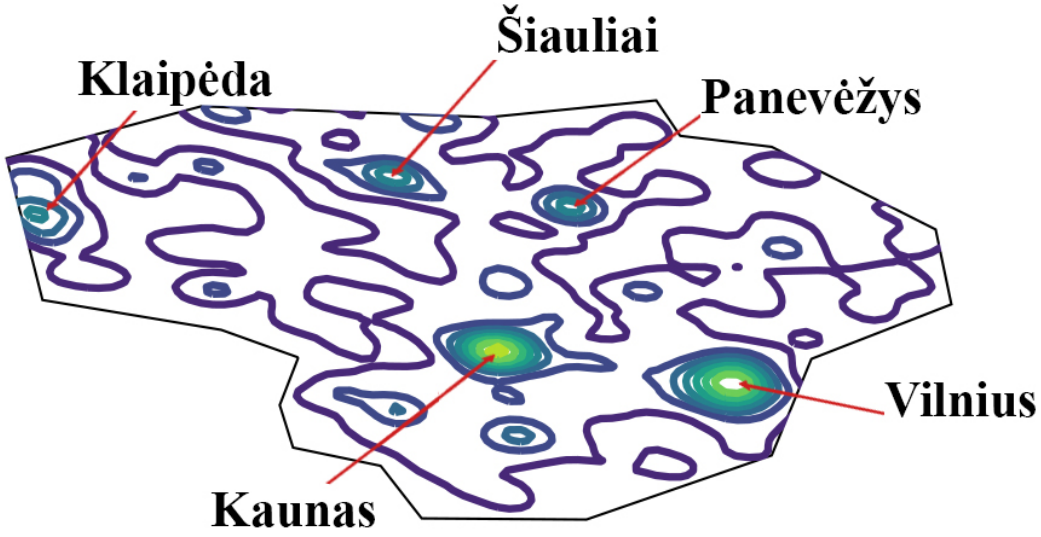

Figure 6: Kernel density plot of the detected buildings.

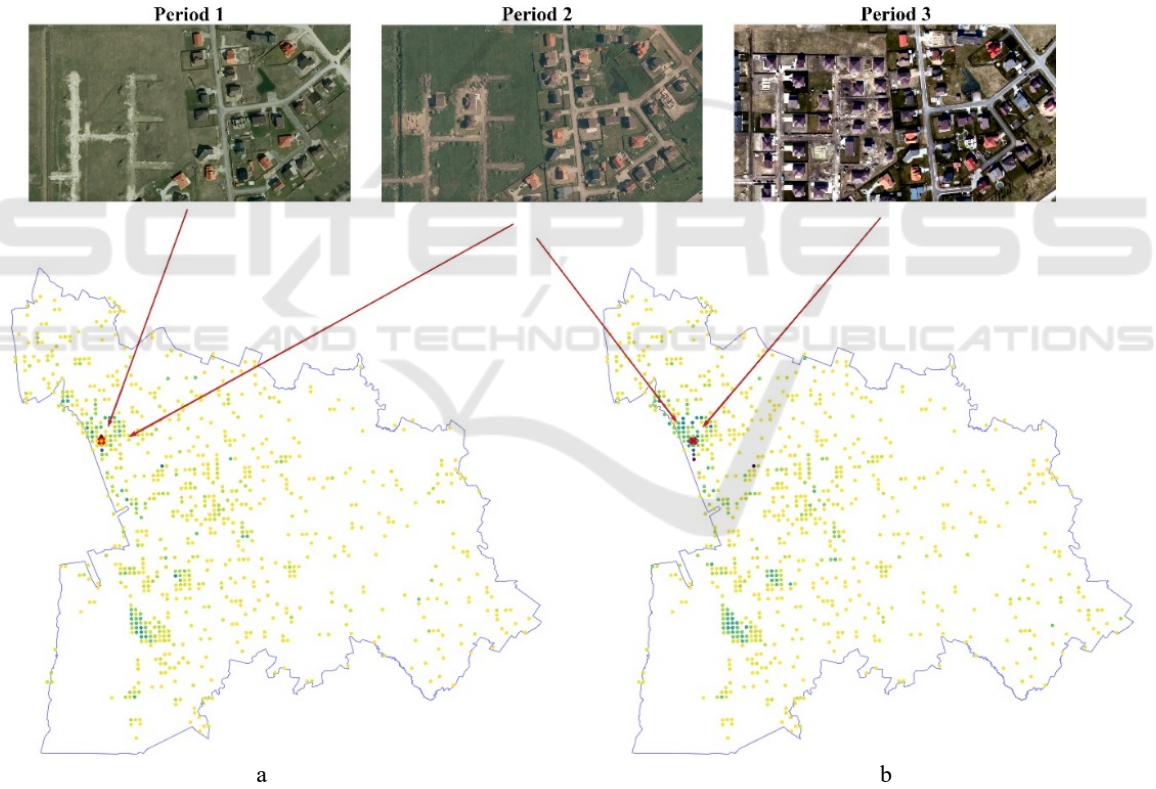

Figure 7: Heat map of difference between building detection in different periods in Klaipėda region. a) periods P2 and P1 compared; b) periods P3 and P2 compared.

Fig. 7. represents the heat map of the difference between the periods P2 and P1, and P3 and P2 in Klaipėda region. To provide validity to the heat map, actual images of the areas that have grown the most were provided for each period. By obtaining a higher frequency of remote sensing data and applying the same methodological approach, more precise urban change could be identified. Currently, only 3 periods were analysed; however, if other satellite images were to be collected, more periods could be identified. With the higher frequency of data, future growth patterns could be forecasted.

a) b) c)

Figure 8: a) Original ORTO10LT view; b-c) processed results and transparent original results with processed results of the selected period (in this case, 2009-2010).

a b

Figure 9: a) OSM data of Kaunas city centre; b) processed data of Kaunas city centre of the selected time period (in this case, 2009-2010).

On the finest level, each period has its own layer which can be visualised using standard map software, i.e. QGis, ArcGis, etc. **Fig. 8-9** demonstrate the results obtained with the model using the QGIS software.

4 DISCUSSION AND CONCLUSIONS

Object detection approaches are usually applied to specific problems and small regions (Liu et al., 2020), (Ye et al., 2019), (Wu et al., 2018), (Dornaika et al., 2016), (Vakalopoulou et al., 2015), while on a country level, only a limited amount of research has been conducted (Al-Ruzouq et al., 2017), (Albert et al., 2017), (Jean et al., 2016). Studies, which applied object detection on a country level, were usually focused on the final result rather than the process itself. In this case, our publication fills in the missing gap by providing a methodological approach of how to prepare the training data and reduce the error between the time series of remote sensing data of different quality. Thus, the provided methodological approach can be applied in different countries for aerial or satellite images in order to determine the urban growth patterns. Several issues were identified when analysing the aerial images in a time series, which were caused by the fact that in time, the technical capabilities enable to obtain better quality (i.e. before 2000, visual data for the same region was available only in grey scale compared to the current RBG of 16 bit depth) or valid external data to ensure the ground truth dataset for model training is unavailable altogether. In this work, transfer learning technique has been applied for creating a machine learning model. The initially pre-trained DeepLabv3 model with a ResNet50 backbone trained on the ImageNet data has been selected. The model adjustment was carried out in two steps. Firstly, adjustment was performed on the OSM data with an autogenerated coarse dataset and the final adjustment for each period with the revised data has been applied at the fine-tuning stage. In the dataset preparation stage, it was demonstrated that the neural network using a base dataset such as OSM is capable of making segmentation on a country level; however, expert input is necessary due to the differences in mapping, use of the most recent ground truth data and the assumption that there are not much changes in

data over the years. Moreover, normalisation of the different quality images on spectrum and contrast allows for creating segmented categorical maps of different periods. It enables to analyse and interpret the results on different levels, where both generalised and granular data is available. The generalised results could be used to detect exceptional patterns by using a contour or heat map, while for the granular level analysis, it is possible to review a map on a specific location, so that the experts could better understand and interpret the generalised results.

ACKNOWLEDGEMENT

This research was supported by the Research, Development and Innovation Fund of Kaunas University of Technology (project grant No. PP91L/19).

REFERENCES

Al-Ruzouq, R., Hamad, K., Shanableh, A., & Khalil, M. (2017). Infrastructure growth assessment of urban areas based on multi-temporal satellite images and linear features. *Annals of GIS*, *23*(3), 183–201. https://doi.org/10.1080/19475683.2017.1325935

Albert, A., Kaur, J., & Gonzalez, M. C. (2017). Using convolutional networks and satellite imagery to identify patterns in urban environments at a large scale. *Proceedings of the ACM SIGKDD International Conference on Knowledge Discovery and Data Mining*, *Part F1296*, 1357–1366. https://doi.org/10.1145/3097983.3098070

Celik, T. (2009). Unsupervised change detection in satellite images using principal component analysis and κ-means clustering. *IEEE Geoscience and Remote Sensing Letters*, *6*(4), 772–776. https://doi.org/10.1109/LGRS.2009.2025059

Corbane, C., Syrris, V., Sabo, F., Pesaresi, M., Soille, P., & Kemper, T. (2020). Convolutional Neural Networks for Global Human Settlements Mapping from Sentinel-2 Satellite Imagery. *ArXiv*.

de Jong, K. L., & Sergeevna Bosman, A. (2019). Unsupervised Change Detection in Satellite Images Using Convolutional Neural Networks. *2019 International Joint Conference on Neural Networks (IJCNN)*, *July*, 1–8. https://doi.org/10.1109/ijcnn.2019.8851762

Donaldson, D., & Storeygard, A. (2016). The view from above: Applications of satellite data in economics. *Journal of Economic Perspectives*, *30*(4), 171–198. https://doi.org/10.1257/jep.30.4.171

Dornaika, F., Moujahid, A., El Merabet, Y., & Ruichek, Y. (2016). Building detection from orthophotos using a machine learning approach: An empirical study on image segmentation and descriptors. *Expert Systems with Applications*, *58*, 130–142. https://doi.org/10.1016/j.eswa.2016.03.024

Goyette, N., Jodoin, P.-M., Porikli, F., Konrad, J., & Ishwar, P. (2012). A new change detection benchmark dataset. *IEEE Workshop on Change Detection (CDW'12) at CVPR'12*, 1–8.

Jean, N., Burke, M., Xie, M., Davis, W. M., Lobell, D. B., & Ermon, S. (2016). Combining satellite imagery and machine learning to predict poverty. *Science*, *353*(6301), 790–794. https://doi.org/10.1126/science.aaf7894

Kanagamalliga, S., & Vasuki, S. (2018). Contour-based object tracking in video scenes through optical flow and gabor features. *Optik*, *157*, 787–797. https://doi.org/10.1016/j.ijleo.2017.11.181

Krupinski, M., Lewiński, S., & Malinowski, R. (2019). *One class SVM for building detection on Sentinel-2 images*. *1117635*(November 2019), 6. https://doi.org/10.1117/12.2535547

Längkvist, M., Kiselev, A., Alirezaie, M., & Loutfi, A. (2016). Classification and segmentation of satellite orthoimagery using convolutional neural networks. *Remote Sensing*, *8*(4). https://doi.org/10.3390/rs8040329

Liu, Y., Han, Z., Chen, C., DIng, L., & Liu, Y. (2020). Eagle-Eyed Multitask CNNs for Aerial Image Retrieval and Scene Classification. *IEEE Transactions on Geoscience and Remote Sensing*, *58*(9), 6699–6721. https://doi.org/10.1109/TGRS.2020.2979011

Marmanis, D., Galliani, S., Schindler, K., Zurich, E., Marmanis, D., Wegner, J. D., Galliani, S., Schindler, K., Datcu, M., & Stilla, U. (2016). *Semantic Segmentation Of Aerial Images With An Ensemble Of CNNS 3D reconstruction and monitoring of construction sites using LiDAR and photogrammetric point clouds View project Earth Observation Image Librarian (EOLib) View project SEMANTIC SEGMENTATION O*. *III*(July), 12–19. https://doi.org/10.5194/isprsannals-III-3-473-2016

Nahhas, F. H., Shafri, H. Z. M., Sameen, M. I., Pradhan, B., & Mansor, S. (2018). *Deep Learning Approach for Building Detection Using LiDAR – Orthophoto Fusion*. *2018*.

Shermeyer, J., & Van Etten, A. (2019). *The Effects of Super-Resolution on Object Detection Performance in Satellite Imagery*. http://arxiv.org/abs/1812.04098

Suraj, P. K., Gupta, A., Sharma, M., Paul, S. B., & Banerjee, S. (2018). *On monitoring development indicators using high resolution satellite images*. 1–36. http://arxiv.org/abs/1712.02282

Vakalopoulou, M., Karantzalos, K., Komodakis, N., & Paragios, N. (2015). Building detection in very high resolution multispectral data with deep learning features. *International Geoscience and Remote Sensing Symposium (IGARSS)*, *2015-Novem*, 1873–1876. https://doi.org/10.1109/IGARSS.2015.7326158

Verbesselt, J., Hyndman, R., Newnham, G., & Culvenor, D. (2010). Detecting trend and seasonal changes in satellite image time series. *Remote Sensing of*

Environment, *114*(1), 106–115. https://doi.org/10.1016/j.rse.2009.08.014

Verbesselt, J., Zeileis, A., & Herold, M. (2012). Near real-time disturbance detection using satellite image time series. *Remote Sensing of Environment*, *123*, 98–108. https://doi.org/10.1016/j.rse.2012.02.022

Wang, B., Tang, S., Xiao, J. Bin, Yan, Q. F., & Zhang, Y. D. (2019). Detection and tracking based tubelet generation for video object detection. *Journal of Visual Communication and Image Representation*, *58*, 102–111. https://doi.org/10.1016/j.jvcir.2018.11.014

Wang, J., Song, J., Chen, M., & Yang, Z. (2015). Road network extraction: a neural-dynamic framework based on deep learning and a finite state machine. *International Journal of Remote Sensing*, *36*(12), 3144–3169. https://doi.org/10.1080/01431161.2015.1054049

Witwit, W., Zhao, Y., Jenkins, K., & Zhao, Y. (2017). Satellite image resolution enhancement using discrete wavelet transform and new edge-directed interpolation. *Journal of Electronic Imaging*, *26*(2), 023014. https://doi.org/10.1117/1.jei.26.2.023014

Wu, G., Shao, X., Guo, Z., Chen, Q., Yuan, W., Shi, X., Xu, Y., & Shibasaki, R. (2018). Automatic building segmentation of aerial imagery usingmulti-constraint fully convolutional networks. *Remote Sensing*, *10*(3), 1–18. https://doi.org/10.3390/rs10030407

Wurm, M., Stark, T., Zhu, X. X., Weigand, M., & Taubenböck, H. (2019). Semantic segmentation of slums in satellite images using transfer learning on fully convolutional neural networks. *ISPRS Journal of Photogrammetry and Remote Sensing*, *150*(December 2018), 59–69. https://doi.org/10.1016/j.isprsjprs.2019.02.006

Xie, M., Jean, N., Burke, M., Lobell, D., & Ermon, S. (2016). Transfer learning from deep features for remote sensing and poverty mapping. *30th AAAI Conference on Artificial Intelligence, AAAI 2016*, 3929–3935.

Ye, Z., Fu, Y., Gan, M., Deng, J., Comber, A., & Wang, K. (2019). Building extraction from very high resolution aerial imagery using joint attention deep neural network. *Remote Sensing*, *11*(24), 1–21. https://doi.org/10.3390/rs11242970